

Comparisons of Love wave amplitude decay for colocated rotation and translation measurements

Bryant Chow,^{1*} Joachim Wassermann,¹ Bernhard Schuberth,¹
Céline Hadziiannou,^{1,2} Stefanie Donner^{1,3} and Heiner Igel¹

¹ Department of Earth and Environmental Sciences, Ludwig-Maximilians-University Munich, Theresienstraße 41, D-80333 Munich, Germany.

² Department of Earth Science, University of Hamburg, Bundesstraße 55, D-20146 Hamburg, Germany

³ Federal Institute for Geosciences and Natural Resources, Stilleweg 2, D-30655 Hannover, Germany

E-mail: bryant.chow@vuw.ac.nz

SUMMARY

The broad-band surface wave magnitude equation assigns magnitude based on station-receiver distance and peak surface wave amplitude. It is standard practice to use the vertical component of peak ground velocity, so that only contributions from the vertical component of Rayleigh waves are present in the surface wave train. With the advent of rotational ground motion data from instruments such as ring laser gyroscopes and fiber-optic gyroscopes, it is possible to consistently measure peak amplitudes of rotations about three orthogonal axes for transient seismic waves. In the surface wave train, observations of vertical rotations are theoretically only sensitive to the transverse nature of Love waves, unaffected by either component of Rayleigh waves. We use this concept to study the amplitude decay of rotations versus translations, and determine the necessity of separate surface wave magnitude equations for Love and Rayleigh waves. Utilizing a large database of recorded seismic events of colocated translations and rotations, collected in Wettzell, Germany, we empirically define new magnitude scales for multiple measured observables: rotation rate, rotation, vertical velocity and transverse velocity. Results indicate that rotation amplitudes decay faster over distance compared to velocity amplitudes, and that the current surface wave magnitude equation is insufficient for predicting the amplitudes of either observable. Synthetic seismograms were produced using Specfem3D Globe on a full scale 3D global model with realistic crustal structuring to compare against observations. Findings suggest that the current global models available for forward simulation are inadequate for accurately predicting amplitudes, and recreating the observed amplitude decay of both translations and rotations.

Key words: magnitude, rotational motions, amplitude decay, surface waves

1 INTRODUCTION

For over a decade, the application of ring laser gyroscope technology to the field of seismology has allowed for near-continuous and direct measurements of rotational ground motions. An ever growing number of observations from seismic events of varying size, distance and source mechanism, has been collected in an expansive catalog of waveform recordings for both direct rotation, and colocated translation measurements. Previous work on this unique waveform dataset includes phase comparisons of translations and rotations with estimations of horizontal phase velocities (Igel

et al., 2005), automatic standardized processing of rotation and translation data (Salvermoser et al., 2017), and variations of surface wave energy in oceanic microseisms (Tanimoto et al., 2016). Much of this preceding work however, focuses on single events, or collections of non-earthquake sources.

In this paper, we aim to characterize and understand the differences in amplitude decay behavior of rotational and translational ground motion for a large number of seismic events. To do this, we make use of a sizeable catalog of earthquake data, as measured by an observatory based ring laser gyroscope, and colocated broadband translation sensor. By processing rotation and translation observations in a near identical manner, we hope to directly compare results over a large set of event magnitudes, epicentral distances and azimuths. We additionally seek to use this information to bet-

* Now at Victoria University of Wellington, School of Geography, Environment and Earth Sciences, Cotton Building, Gate 7 Kelburn Parade, Wellington, New Zealand 6012

2 Bryant Chow

ter understand decay characteristics of Love and Rayleigh waves.

This paper builds on results previously shown by Igel et al. (Igel et al., 2007), where the question was posed: whether observed peak rotation amplitudes matched with expected values given by the surface wave magnitude equation. As a relatively new observable, rotational ground motion does not share the historical robustness that translations have, for example there exist no empirical relationships such as magnitude equations, which are constantly referred to in seismology. It is therefore important to re-establish these relationships, and in doing so determine whether divergence is required, or if the new observable behaves similarly. At the time of Igel et al. (Igel et al., 2007), a limited number of recorded events lead to a small sample size. With a much larger number of events now currently available, we attempt to readdress this question, while also approaching the problem from the unique perspective of deriving magnitude scales to quantify and compare the decay characteristics of rotations and translations. Due to the uniqueness of our instrumental setup, we are restricted to single station observations. In order to provide comparisons to our observations, global 3D synthetic simulations were run with the wave propagation code Specfem 3D Globe (Komatitsch and Tromp, 2002a) (Komatitsch and Tromp, 2002b). Real seismic event locations, source parameters, and station locations are used, in order to provide the most comparable synthetic setup to observations.

With these observations, we aim to make quantitative statements on surface wave amplitude decay, as well as to provide magnitude scale equations that may prove useful in determining expected rotation amplitudes from seismic events.

1.1 Rotational Ground Motions

To fully describe rigid body motion at a point, three components of translation, and three components of rotation must be defined (Stein and Wysession, 2009). In seismology, standard practices make use of translation only, which means recorded motions only approximate the rigid body motion, and can potentially be polluted by rotational signals which cannot be separated from physical effects (Igel et al., 2005), (Aki and Richards, 2002). Rotational ground motions induced by seismic events can currently be observed through direct measurement, and through array analysis of translation sensors (Spudich et al., 1995). In the latter, spatial gradients are taken between instruments in adequately spaced array of translation sensors, in order to derive components of the strain tensor. Shortcomings of array based methods, however, include the necessity for multiple sensors and careful consideration for array spacing and geometry. With unique instrument designs, however, direct gradient measurements from a single instrument are possible (Schreiber et al., 2006a).

Observations for this study were recorded by the GroBring (G-ring) (Schreiber et al., 2006a) (Schreiber et al., 2006b), a 4x4m helium-neon ring laser gyroscope, located at the Geodetic Fundamentalstation in Wettzell, Germany (49.144°N , 12.87°E). The G-ring operates on the principle of Sagnac interferometry (Stedman, 1997), which relates in-

terference of counter propagating light beams to absolute rotation rate, through the following equation,

$$\delta f = \frac{4A}{\lambda P} \mathbf{n} \cdot \hat{\boldsymbol{\Omega}}, \quad (1)$$

where the constants are given by instrument area A, perimeter P and operating light wavelength λ . Equation 1 relates an observable beat frequency δf [Hz] to absolute rotation rate Ω [rad/s].

It is important to note that given stable instrument geometry and lasing, changes to the beat frequency δf , can only be introduced by changes to the inner product of the plane normal \mathbf{n} with the rotation rate direction $\hat{\boldsymbol{\Omega}}$ (e.g. through instrumental tilt), and through externally induced rotations (e.g. the passing of seismic waves). It has been shown that changes to the inner product as produced by tilt are one to two orders of magnitude smaller than rotations produced by passing seismic waves (McLeod et al., 1998) (Schreiber et al., 2006a) (Schreiber et al., 2006b), this provides the unique benefit that the G-ring (and other instruments operating on this principle) is theoretically insensitive to translations.

1.1.1 Phase velocity relation

It has been shown that for a simple plane wave, the amplitudes of vertical rotation rate Ω_z and transverse acceleration \ddot{u}_t can be related through the equation

$$\frac{\ddot{u}_t}{\Omega_z} = -2c, \quad (2)$$

where c represents an apparent horizontal phase velocity (Igel et al., 2005); given a sufficient event-receiver distance (allowing a plane wave assumption), measured rotations are sensitive to the transverse component of translation, represented in teleseismic waves by surface horizontal waves (i.e. SH or Love waves). Equation ?? also shows that waveforms of transverse acceleration and vertical rotation rate should theoretically be in phase, with oppositely polarized amplitudes, for passing horizontal waves. This can be seen in Figure 1, showing two superimposed traces of rotation rate and transverse acceleration (filtered at $T=20$ s) for G and a colocated broad band seismometer (top) and synthetically generated seismograms (bottom) [!!! ADD EVENT INFORMATION]. For the observations, following Equation ??, a value of 3.81 km/s is calculated for the horizontal phase velocity, which matches well with previous findings of phase velocity from rotational studies for this area (Igel et al., 2007).

1.1.2 Peak correlation coefficient

Correlations are a useful measure of similarity between two signals. It has been shown previously that for collocated measurements of vertical rotation rate and transverse acceleration, high values (> 0.9) of zero lag correlations can be obtained in time windows centered around S-wave, or surface wave, arrivals (Igel et al., 2007). Zero lag correlation coefficients are routinely computed for events measured by G (Salvermoser et al., 2017), and are used in this study as a

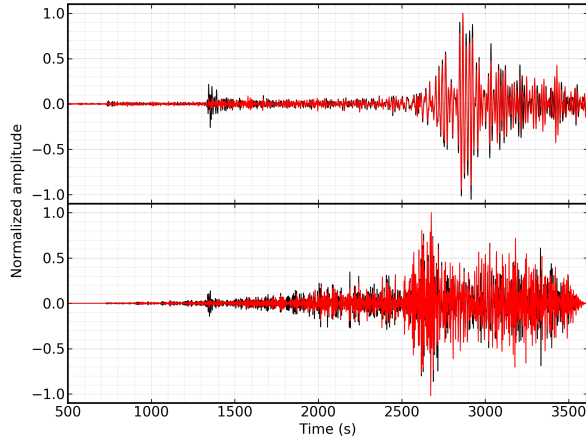


Figure 1. Comparisons of rotation and translation. Observation (top) and synthetic (bottom) seismograms for an M_w 6.67 event near Japan (see Table 1). Waveforms filtered at 5 to 60 seconds. Red traces show rotation rate, black traces show transverse acceleration, amplitudes normalized from zero to one. Calculating for horizontal phase velocity with peak amplitudes using Equation 2 gives $c_{obs} = 3.52$ and $c_{syn} = 3.95$ for observations and synthetics, respectively.

filtering tool to highlight "bad" events that exhibit low signal to noise ratios, or dissimilar waveforms which may arise due to non-physical effects (e.g. instrumental effects). Here, the largest correlation coefficient obtained for a seismogram is labeled the peak correlation coefficient (PCC), and is used as a representation of data quality.

1.2 Magnitude scales

Amplitude based magnitude scales provide empirically derived relationships between maximum trace amplitudes and source-receiver distances. Magnitude scales offer useful and quick estimates of relative sizes of earthquakes in a simple, standard manner. The International Association of Planets Seismology and Earth's Interior (IASPEI) Working Group on Magnitudes proposed a modified version of the original surface wave magnitude equation (Prague formula), proposed by (Karnik et al., 1962). This broad band surface wave magnitude equation is compatible for use with modern day broadband seismic instruments (Bormann and Bergman, 2000).

In this work, we adhere strictly to the standard procedures provided by IASPEI (outlined in the following section) as a stencil for defining our own empirical magnitude scales. In turn, we use these derived scales as a tool for quantifying amplitude decay for different measured observables.

1.2.1 Standard Procedures

The Working Group on Magnitudes' standard procedures gives the revised surface wave magnitude equation for broadband instruments as,

$$M_S^{BB} = \log_{10}(V/2\pi) + B \cdot \log_{10}(\Delta) + C, \quad (3)$$

where the constants $B = 1.66$ and $C = 0.3$ control amplitude decay and order of magnitude, respectively. The parameter V should be the maximum trace amplitude (in nanometers second $^{-1}$) in the surface wave train, for a seismogram proportional to velocity, measured on the vertical component.

Further criteria given by IASPEI posit that the period of the surface wave should lie within $3 \text{ s} \leq T \leq 60 \text{ s}$, while epicentral distances should be between $2^\circ \leq \Delta \leq 160^\circ$. It is further recommended that only shallow focus earthquakes should be considered, as medium to deep events are less capable of generating strong surface waves. Maximum trace amplitudes are described as one half the largest peak to adjacent trough deflection, and associated period are given as two times the temporal difference between peak and adjacent trough. All events and processing steps in this paper adhere to these guidelines.

1.2.2 Instrumental proxies for Love and Rayleigh waves

A standard procedure for determining surface wave magnitude scales is to take amplitudes measured on the vertical component of translation. This is because vertical translation should only be sensitive to the vertical motions of Rayleigh waves, whereas vector sums of horizontal components can be influenced by both Love and Rayleigh waves. In the same vein, velocity measured on the transverse component should only show sensitivity to Love waves (and radial components should only be sensitive to the horizontal component of Rayleigh waves). It is not common practice to use transverse components in calculating magnitude, due to the necessity of rotating horizontal components to the correct azimuth, which can be affected by ray paths, local site effects and correct epicenter location. The G-ring, which is 1) insensitive to translations and 2) proportional in phase and amplitude to transverse acceleration, should only be sensitive to Love waves in the surface wave train, irrespective of azimuth.

In this study we use our instruments as physical wave-filters, in order to study individual phases in the surface wave train. This allows us to analyze the influences of Love waves and Rayleigh waves separately. By comparing the vertical and transverse components of translations, to the vertical component of rotation, we can understand, by proxy, the wave types they are sensitive to.

1.2.3 Application of rotations to magnitude scales

In order to give a fair comparison to translations using derived magnitude scales, a rotation parameter complementary to velocity is necessary. In Section 1.1.1, an equation is given that relates rotation rates Ω with accelerations $\ddot{\boldsymbol{u}}$. It would make the most sense, then, to compare velocities $\dot{\boldsymbol{u}}$ with rotations $\boldsymbol{\omega}$ (by integrating both sides). However, without previous work to draw precedence from, and for completeness, we present observations of both rotations and rotation rates in this study.

2 EVENT CHOICE

The G-ring has been continuously recording at its current resolution since May, 2009 (Salvermoser et al., 2017). Events

4 Bryant Chow

used in this study span from June 1, 2009 to September 1, 2016. An initial earthquake catalog was fetched from the Harvard Global Centroid Moment Tensor (GCMT) (Ekström et al., 2012), with events filtered by acceptable magnitude, source depth and epicentral distance from Wettzell, Germany. At this point we imposed the restriction that the derived "magnitude" as given by our magnitude equations, should fall as close to the given surface wave magnitude as possible. This ensures that our derived scales do not stray too far from established scales. Consequently we only consider events with published centroid moment magnitude values of $6 \leq M_{wc} < 8$; surface wave magnitude and moment magnitude are approximately equal in this range (Shearer, 2009). Zero-lag cross correlations of transverse acceleration and rotation rate were taken in order to calculate peak correlation coefficients (Section 3.1). Events were not considered if their peak correlation coefficient did not meet the criterion $PCC \geq 0.7$.

These choices for event criteria narrowed the catalog down to roughly 500 events. Each event was appropriately filtered and processed (Section 3.1), and waveforms were individually inspected. Waveforms that exhibited anomalous behavior (e.g. unexpected high amplitude peaks outside the surface wave train, high signal-to-noise ratio etc.) were rejected. A final event catalog of 243 events was reached, shown in Figure 2.

3 METHODS

3.1 Data Processing

Events were processed in a similar fashion as the processing outlined in Salvermoser et al. (Salvermoser et al., 2017). Raw, continuous translation data in North, East and vertical components, as well as vertical rotation rate data, was fetched based on event origin time. Instrument response correction produced translation seismograms proportional to units of velocity (nm s^{-1}). Epicentral distances (Δ) and theoretical backazimuth values were calculated from station-receiver latitude longitude pairs, and events were separated into categories of close ($\Delta < 3^\circ$), local ($\Delta < 100^\circ$) and far ($\Delta \geq 100^\circ$). Translations were rotated into the transverse, radial, vertical coordinate system by the appropriate theoretical backazimuth. Measurements from ring laser gyroscope instruments do not require frequency dependent instrument correction (Schreiber et al., 2006a), therefore only a simple scale factor was necessary to retrieve seismograms proportional to rotation rate (nrad s^{-1}).

Rotation rate traces were integrated to provide measurements of rotation (nrad), and transverse velocity was integrated to retrieve transverse acceleration, which was subsequently used to calculate correlations with vertical rotation rates. A bandpass filter was applied to all traces for periods between $3 \text{ s} \leq T \leq 60 \text{ s}$, in accordance to the IASPEI standard procedures. Peak amplitudes were chosen by finding minimum and maximum trace values and the largest associated peak or trough, respectively. The larger of the two was recorded, alongside the associated arrival time and dominant period, taken as two times the distance between peak and adjacent trough.

Theoretical considerations were initially used to restrict

search to the surface wave train, however results proved inconsistent, so maximum amplitudes in the entire trace were considered. Through manual inspection, picked amplitudes that fell outside the surface wave train (which occurred very infrequently) were rejected. An example of the waveform and amplitude picking is shown in Figure 3.

3.1.1 Zero-lag correlations

To calculate peak correlations, traces of transverse acceleration and vertical rotation rate were segmented into small time windows based on the event-station distance. In each time window, a zero-lag correlation was performed, and a single value of correlation produced. From the entire trace, the max value was taken to represent the peak correlation coefficient. For most waveforms, the peak correlation coefficient lies in the surface wave train. As mentioned previously, these peak correlation values are used extensively as a ranking system for events, providing a quickly attainable measure of waveform quality.

3.2 Curve fitting

To quantify amplitude decay, magnitude scale coefficients were fit to the data using a simple linear regression. Using the general form of the magnitude equation, given by Equation 3, a collection of n events can be represented in the form,

$$\begin{pmatrix} \log_{10}(\Delta_1) & 1 \\ \log_{10}(\Delta_2) & 1 \\ \vdots & \vdots \\ \log_{10}(\Delta_n) & 1 \end{pmatrix} \begin{pmatrix} B \\ C \end{pmatrix} = \begin{pmatrix} M_{wc_1} - \log_{10}(V_1/2\pi)_{\max} \\ M_{wc_2} - \log_{10}(V_2/2\pi)_{\max} \\ \vdots \\ M_{wc_n} - \log_{10}(V_n/2\pi)_{\max} \end{pmatrix}, \quad (4)$$

which can be expressed in the matrix-vector form, $\mathbf{G}\mathbf{m} = \mathbf{d}$. The unknowns B and C are represented in the vector \mathbf{m} , and can be solved for through the normal equation $\mathbf{m} = (\mathbf{G}^T \mathbf{G})^{-1} \mathbf{G}^T \mathbf{d}$. By solving for the vector \mathbf{m} , we create an empirical magnitude scale that best describes the amplitude decay behavior of our observations. In Equation 4, we impose that our derived magnitude value should be as close to the given moment magnitude as possible, by setting M_S^{BB} equal to the value of M_{wc} retrieved from our event catalog.

Confidence intervals were constructed for each parameter of the vector \mathbf{m} . These were calculated with the variance of estimates of the j th parameter of \mathbf{m} by the equation $\hat{m}_j \pm c \sqrt{\hat{v}ar(\hat{m}_j)}$, where the value of c is given as 1.96 for a confidence interval of $\alpha = 0.95$. [more explanation of confidence intervals needed]

4 SYNTHETIC SEISMOGRAMS

Due to the unique instrumental setup of the G-ring, there are currently no other datasets to draw comparisons against. It should be mentioned that there are other available rotation instruments which have been used for earthquake analyses (Donner et al., 2017), (Sbaa et al., 2017), however they lack any substantial earthquake catalog. One possibility for gathering more observations would be through array derived rotations as a substitute for direct rotation measurements;

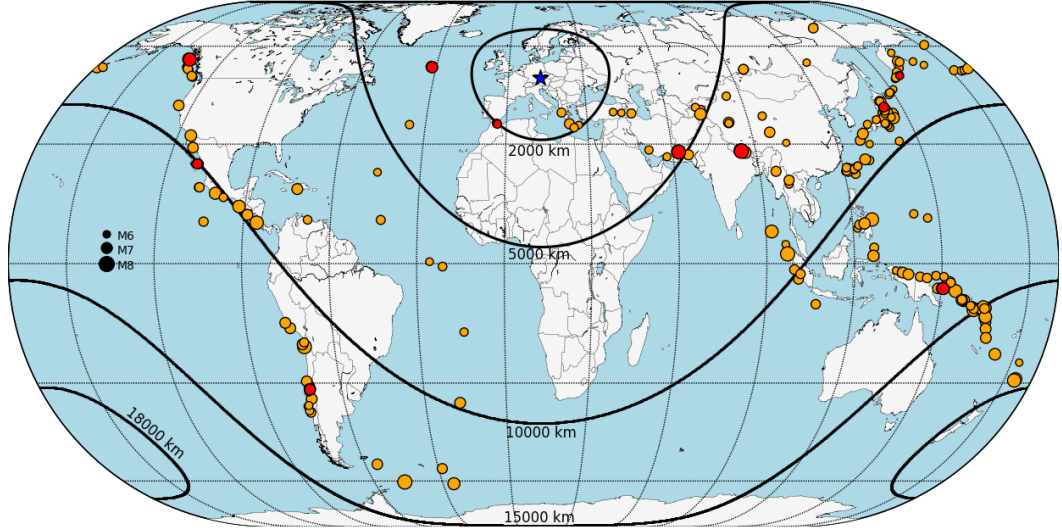


Figure 2. Event map. Size represents moment magnitude (M_{wc}). Orange dots show observed earthquakes used in magnitude scale derivation. Red dots show the ten events chosen for generation of synthetic seismograms. Black lines are equidistant points from the blue star, which represents the location of G in Wettzell, Germany ($49.144^{\circ}\text{N}, 12.87^{\circ}\text{E}$).

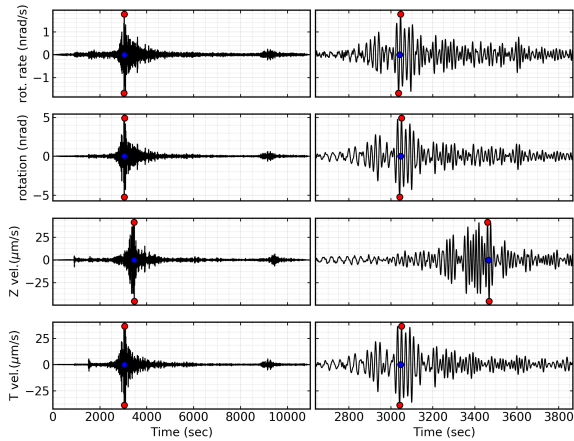


Figure 3. Peak amplitude picking. Left column shows seismograms of the 2011 M_w 6.67 event (See Table 3). From top to bottom: rotation rate, rotation, vertical velocity, transverse velocity. Red dots show largest peak to peak. Blue dots shows zero crossing for the chosen peak to peak amplitude. Right column shows zoomed in section of respective seismograms. Note the visible difference in amplitude picks of the Love wave and the later arriving Rayleigh wave.

this option was noted during analysis, however it proved difficult finding sufficient long-term arrays with optimal station spacing. If this type of data became available or accessible, it would provide a very useful addition of information. In lieu of this, we turn to waveform modeling to generate synthetic seismograms, with which we recreate our experimental setup to provide a comparable set of synthetic observations.

The seismic wave propagation code Specfem3D Globe was employed. A realistic global model featuring 3D crust (crust2.0 (Bassin et al., 2000)) and mantle (S40RTS (Ritsema et al.,)) models was used. The simulation featured effects that might have potential influence on surface waves at the periods of interest, which include: ocean loading, Earth ellipticity, topography, self gravitation, Earth's rotation and 1-D attenuation. Event locations and moment tensors were taken from 10 real seismic events present in the observation catalogs. Events were chosen based on values of peak correlation coefficients, as well as optimal event location and depth, so as to provide a varied distribution of source-receiver pairings. Table 1 provides detailed information on the chosen events.

In each simulation, events were initiated as point sources. The simulation corner frequency was set to 10 seconds, and simulations were run for one hour simulation time. As computational cost is independent of number of stations, more than one hundred stations were included; station locations were taken from Global Seismic Network (GSN) locations, with the addition of the G-ring, and the German observatory station Fürstenfeldbruck ($48.163^{\circ}\text{N}, 11.275^{\circ}\text{E}$), which was used for comparisons in observations.

5 RESULTS

5.1 Derived magnitude scales

Decay characteristics of rotations and translations were derived by solving for constants B and C in Equation 4. The values for each scale are presented in Table 2. For an additional check on site-dependent data quality, the same analysis was performed on translation observations taken at the geophysical observatory Fürstenfeldbruck, Germany (FUR; $48.163^{\circ}\text{N}, 11.275^{\circ}\text{E}$), located roughly 200 km south-west of Wettzell. Though a smaller subset of events was used due to data availability, the results confirmed those given at Wettzell.

The value of B covers a large range, from 1.084 to 1.823 for vertical velocity M_Z^{WET} and rotation rate M_{RR}^{RLAS} , re-

Date	Time (UTC)	Lat($^{\circ}$)	Lon($^{\circ}$)	Depth(km)	Δ ($^{\circ}$)	M_{wc}	Flinn-Engdahl Region
2010-07-18	13:34:59	-5.93	150.59	35.0	124.3	7.32	New Britain Region, P.N.G.
2011-09-16	19:26:41	40.27	142.78	35.0	80.8	6.67	Off East Coast Of Honshu, Japan
2013-01-05	08:58:19	55.39	-134.65	10.0	72.1	7.53	Southeastern Alaska
2013-04-16	10:44:20	28.03	62.0	80.0	43.2	7.74	Southern Iran
2013-04-19	19:58:40	49.97	157.65	15.0	76.8	6.06	East Of Kuril Islands
2015-02-13	18:59:12	52.65	-31.9	16.7	28.6	7.07	Reykjaness Ridge
2015-04-25	06:11:26	28.15	84.71	15.0	58.3	7.88	Nepal
2015-09-13	08:14:12	25.14	-109.43	10.0	90.1	6.6	Gulf Of California
2015-09-16	23:18:41	-31.56	-71.43	28.4	110.3	7.1	Near Coast Of Central Chile
2016-01-25	04:22:02	35.65	-3.68	12.0	18.2	6.38	Strait Of Gibraltar

Table 1. List of events used as synthetic sources in Specfem3D. Events were chosen based on a diverse coverage of magnitudes and epicentral distances (Δ) from the ring laser stationed in Wettzell, Germany. Event information taken from the GCMT catalog.

spectively. Rotation M_{RT}^{RLAS} falls closest to the standard IASPEI value of $B=1.66$. Velocity values match quite consistently between Wettzell and Fürstenfeldbruck, with FFB showing slightly higher amplitudes, as seen in the value of C, which controls the order of magnitude of expected amplitudes. In comparing these two stations, consideration should be given to the subsurface composition; the geodetic observatory in Wettzell overlies granitic bedrock, while Fürstenfeldbruck sits atop a sedimentary basin, which are known to amplify passing seismic waves (i.e. (Rial et al., 1992)). It would therefore not be surprising to observe on-average larger amplitudes at Fürstenfeldbruck. Larger amplitudes are visible in the transverse component of FFB relative to WET, seen in Figure 5, however the vertical component does not reflect this.

Variations of velocity based scales from the surface wave magnitude equation are large, but not entirely unexpected. It has been proposed that the surface wave magnitude equation has a systematic distance bias, which tends to under predict amplitudes at greater distances (Herak and Herak, 1993). Previous works have proposed corrected values of the coefficients B and C, using a global catalog (Herak and Herak, 1993) and a European regional dataset (Ambraseys and Free, 1997). These corrections match well with the vertical velocity scales derived in this work; the values (adjusted for the change of units in the IASPEI scale) are presented in Table 2 as M_S^{HH} and M_S^{AF} for corrections proposed by Herak & Herak (Herak and Herak, 1993) and Ambraseys & Free (Ambraseys and Free, 1997), respectively.

There exists a noticeable difference between values of B for transverse and vertical velocities. The vertical velocity scale is expected to present an identical setup to the broad-band surface wave magnitude equation, however it presents the largest discrepancy, for both stations WET and FUR. Transverse velocity, which should sample Love waves, same as rotations (see 1.2.2), shows a larger value for B as compared to vertical velocity.

Confidence intervals, which can be viewed as a quantification of misfit between the magnitude equation we fit and the observations, shows the uncertainty of the observations due to the limitation of spatial coverage; in Figure 4, the red shaded area shows the confidence interval of the M6 decay line. Relatively large uncertainties arise from the large scatter between predicted and expected amplitudes. It should be noted that the magnitude scale is heavily controlled by its end members. Due to a lack of events at very close epicentral

distances, it is difficult to constrain the decay here, and the few events at distances less than 20° have a strong influence on the derived value of B. It can also be seen that more than one third of the events used in this study fall around 80° epicentral distance, due to geographic constraints; many of these events occur around Japan, as seen in Figure 2.

5.2 Observed and synthetic waveforms

For each of the simulated events, synthetic seismograms were generated for all stations mentioned previously. Waveforms for station WET were compared for all possible components of translation and rotation. In one event (2010-07-18), a fore shock in the observations went unnoticed during event choice, which obscured arrivals and prevented useful comparison with synthetics. In most other cases, P-wave and S-wave arrivals matched well. Later arrivals are not in agreement with very different behavior exhibited by arriving surface waves. This can potentially be explained by the use of point sources for such large magnitude earthquakes; the effects of the source time function as well as the rupture plane are not captured in our synthetics, and we therefore do not expect to match phases of surface wave arrivals. Consideration should also be given to the topographic and crustal models included, which affect the resulting surface wave waveforms. The broad frequency range (10-60s) also present difficulties in matching waveforms. Narrow pass filters (i.e. 20 second dominant period) capture similarities better, however we aim to stick to the definition of the IASPEI surface wave magnitude equation, which calls for this broad frequency range. Fortunately in this study, we focus on peak amplitude measurements and therefore are not heavily impacted by the misfit of waveforms.

Comparisons of transverse acceleration and rotation rate provide solid phase matching throughout the waveform, with the strongest correlation during the surface wave train, even for relatively wide bandpass filters (i.e. 10 to 60 seconds). This is true for both observations and synthetics, and also allows for the calculation of phase velocities. Because this is not the goal of this paper, we do not delve too far into the analysis of phase velocities, however taking peak value amplitude ratios for broad bandpass filter ranges (which would average the horizontal phase velocities of each dominant period contained), we recover values ranging from 3 to 5 km/s.

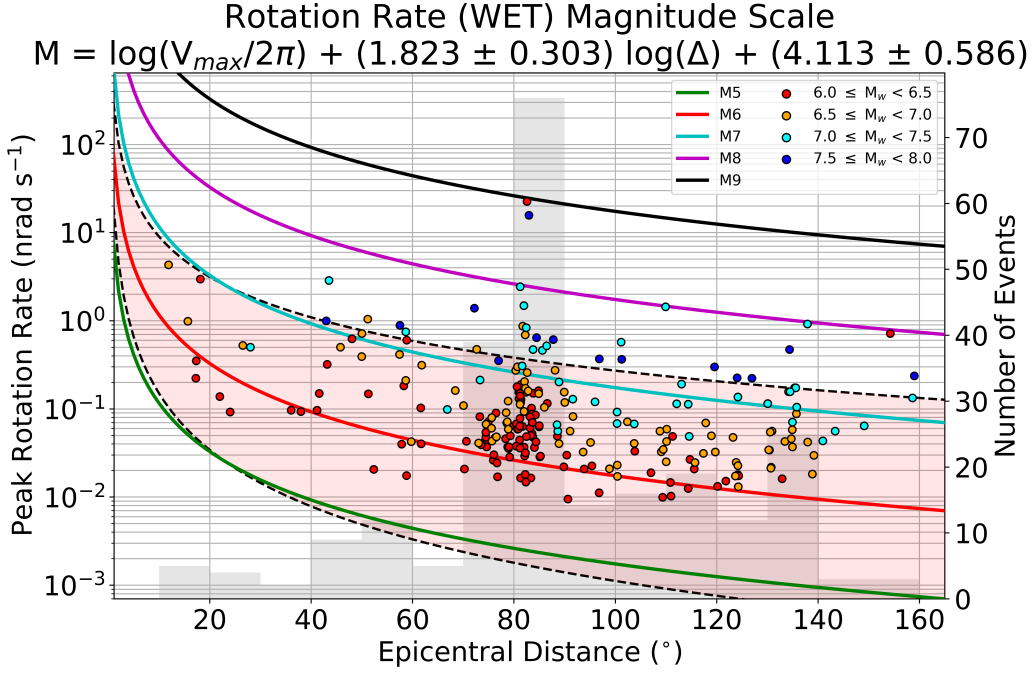


Figure 4. Rotation rate magnitude scale for observations. Event magnitudes separated by bins of 0.5 and denoted by color. Magnitude equation plotted by integer values as solid color lines. 95% confidence interval for M6 shown by the shaded red area, bordered by black dashed lines. The number of events for each epicentral distance bin shown by gray bars in the background.

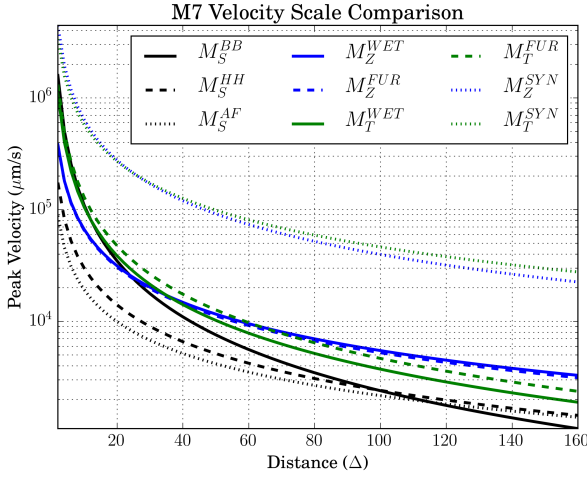


Figure 5. A comparison of velocity based scales for stations WET, FUR and synthetic scales, with the IASPEI scale used as reference. Peak amplitudes given in units of nanometers/s

5.3 Synthetic magnitude scales

Results derived from synthetic seismograms, shown in Table 2, vary quite dramatically from the observations. Synthetic results do not reflect the same discrepancies that are present in the values given by observations.

A visual representation for the synthetic rotation rate magnitude scale M_{RR}^{SYN} is shown in Figure 8. The distribution of points on this scale is much more uniform compared to 4. This can be attributed to the substantially larger number of recordings for a single event due to the large number

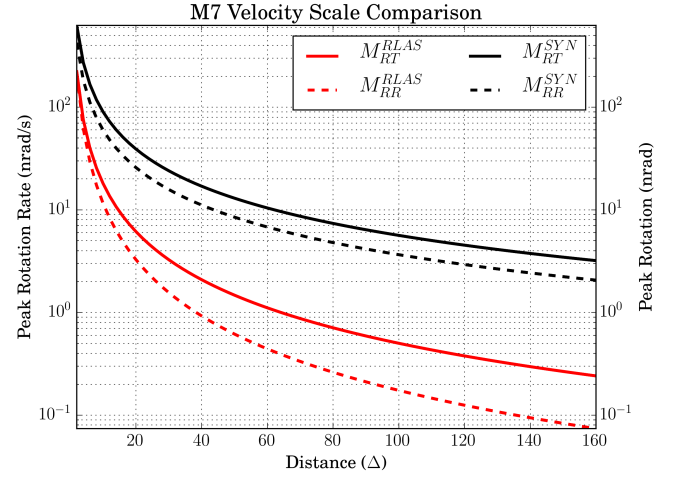


Figure 6. A comparison of rotation based scales for station WET and synthetic scales. Peak amplitudes given in units of nanoradians/s [need to change or remove incorrect figure title]

of synthetic stations. With so many station receiver pairs over a range of epicentral distances, there are roughly six times more observation points, which provides stronger coverage of epicentral distances. The number of events at very close distances is also quite low, similarly due to the imposed geographic limitations. The 95% confidence intervals provide a much narrower band, due to the very consistent spacing of points for a single event; capturing a single event over the entire distance range puts a strong constraint on the fitted decay constants.

The synthetic magnitude scales all exhibit very similar

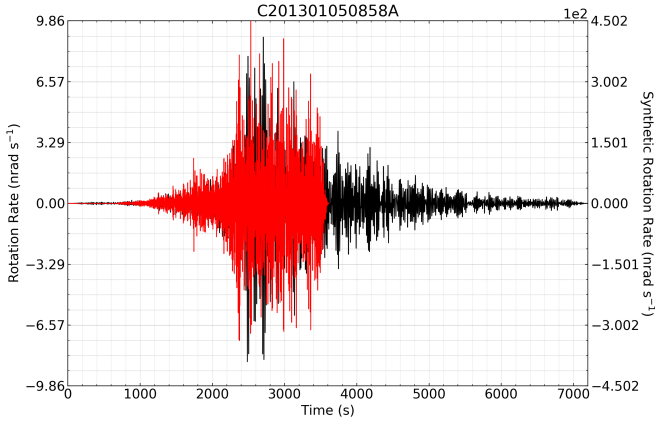


Figure 7. Direct comparison of observed (black) and synthetic (red) rotation seismograms for an M_w 7.53 in Alaska. Note the similarities in waveform, contrasted by the order of magnitude difference in amplitudes.

values for the decay constant B . The large variation seen in the observations is not captured here. Compared to the IASPEI magnitude scale, all values of B for derived synthetic scales fall lower. Synthetic rotation rate gives the largest, or steepest decay constant at 1.215, but only by a negligible margin. Looking at the values of C , expected amplitudes are all also quite high, except for rotation rate.

5.4 Expected rotation amplitudes

One useful aspect of magnitude scales is to provide an expected amplitude value for a given magnitude event at certain distance. One area of interest in rotational seismology is the development of field deployable sensors. Due to the low order of magnitude of rotation amplitudes (teleseisms measured in nanoradian scale), it is of concern whether newly developed field deployable rotation sensors can reach the sensitivity necessary to capture the rotational motion amplitudes excited by regional or tele-seismic events. With the rotational magnitude scale derived here, we are able to create a list of observation-based expected amplitudes. At the time of writing, the field deployable rotation sensor BlueSeis from the company iXBlue, has a noise floor of roughly $1 \text{ nrad/s}/\sqrt{\text{Hz}}$ (Bernauer et al., 2018). Referring to Table 2, the approximate maximum distance the sensor can be placed to detect a $M_w 5$ event would be 21° epicentral distance, roughly 2300 km. This distance range would mean current day sensors could detect regional $>M5$ earthquakes. Other considerations must be taken into account before these values can be used for field deployment decisions, however it provides a useful approximation for future instrument deployments.

6 DISCUSSION

The long term continuous recordings of rotation and translation waveforms at Wettzell has provided an extensive catalog of colocated observations to explore four components of seismic signals, for events of varying source parameters and

travel paths. The motivation for addressing amplitude decays in the initial study of Igel et al. (Igel et al., 2007), was to determine whether or not decay of peak observed rotation rates was consistent with the definition of the commonly used surface wave magnitude equation. In this study we expanded our motivation to include the comparison of decay rates between rotations and translations, to see if, and how, these quantities might differ. Measurements of seismically induced rotation amplitudes have never been addressed on such a scale, and if rotation measurements should someday be incorporated into standard seismological practices, it is useful and beneficial to understand the general characteristics of their observed signals.

The rotation based magnitude scales in Table 2 present the idea that rotation amplitude decay is not exceedingly different from those for translation measurements; that is, values of B are not orders of magnitude different. Since rotation measurements in the surface wave train sample the horizontal nature of the Love wave, this finding is not so surprising, and of course was already shown previously by Igel et al. (Igel et al., 2007). It does prove reassuring that instruments measuring rotation, given the necessary resolution, will not face any differences in recording events at distance.

Although translation measurements exhibit lower values of B , it has been stated previously ((Herak and Herak, 1993)/(Ambraseys and Free, 1997)) that this result is not unexpected, and perhaps even a better representation of the surface wave amplitude decay. The stark contrast between the values of B for scales sensitive to Love waves versus Rayleigh waves is very interesting. Taking theoretical assumptions into account, we can use these results to make the cautious statement that Love waves have a faster amplitude decay rate compared with Rayleigh waves. Granted we are sampling only in one point in space, however the comparisons of an identical catalog of events for these observable paints a striking contrast. This statement is of course made via instrumental proxies. We can strengthen this statement by taking transverse velocity into consideration, which has a value of B that lies closer to that of rotation; determining transverse velocity is dependent on the correct rotation of North and East components, and it is possible that incorrect rotation can lead to mixing of Love waves and the radial component of Rayleigh waves. If radial and vertical components of Rayleigh waves decay at the same rate, this would lead to the effect seen in Table 2: a slightly lower value of B than that of rotation, a scale that is instrumentally insensitive to translations. (A backazimuth value that is incorrect by 10° changes the expected amplitude of the transverse component by 75%. [is this necessary to justify the statement?])

It should be expected that rotation rate shows a larger value for B as compared to rotation, as we compare a quantity with its time derivative, which contains amplified high frequency components and should exhibit faster decay with distance as the wave path filters out the high frequency energy [move to discussion?].

Although moment magnitude has proven a more physical measure of earthquake size, surface wave magnitude is still widely used by agencies around the world; these scales will serve a purpose for time to come, for one because historic seismic events are only comparable in these scales, and

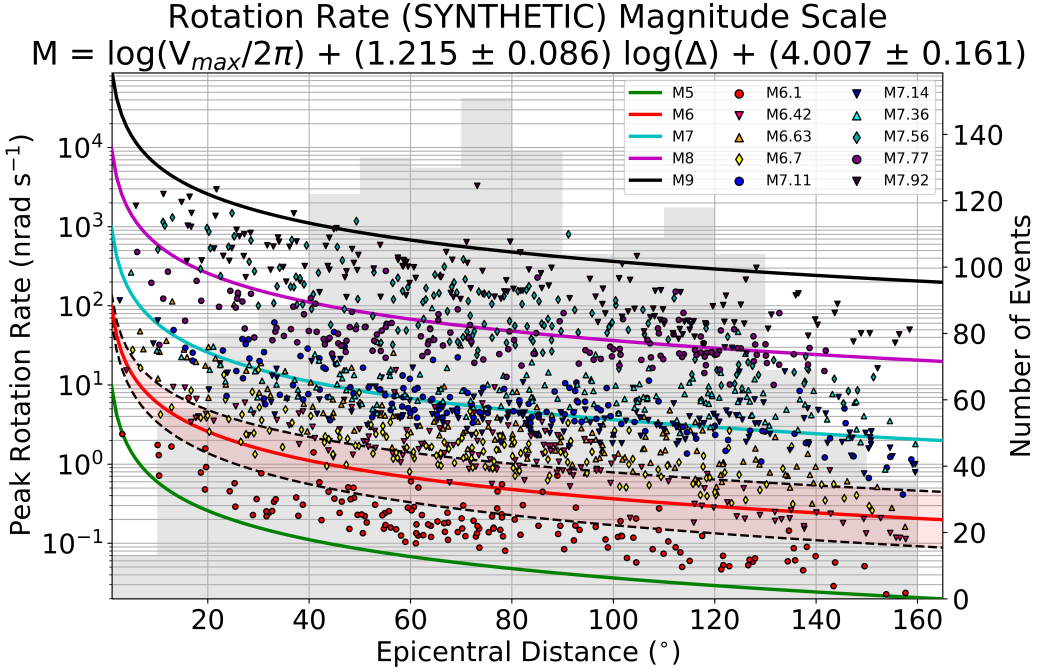


Figure 8. Rotation rate magnitude scale for synthetics. All objects similarly represented as in Figure 4. Colors of points here represent individual events simulated (for event information, see Table 1). Scatter from a perfect decay curve potentially due to the effects of varying travel paths through the 3D crustal and mantle models, amplified by the random distribution of source-receiver pairs.

Scale	Label	B	C	Wave
IASPEI	M_S^{BB}	1.66	0.3	Rayleigh
Herak Herak 1993	M_S^{HH}	1.094	1.429	Rayleigh
Ambraseys-Free 1997	M_S^{AF}	0.947	1.77	Rayleigh
Rotation	M_{RT}^{RLAS}	1.557 ± 0.295	4.186 ± 0.569	Love
Rotation Rate	M_{RR}^{RLAS}	1.823 ± 0.303	4.113 ± 0.586	Love
Transverse Velocity (Wettzell)	M_T^{WET}	1.45 ± 0.27	0.527 ± 0.521	Love
Transverse Velocity (FFB)	M_T^{FUR}	1.442 ± 0.27	0.447 ± 0.523	Love
Vertical Velocity (Wettzell)	M_Z^{WET}	1.084 ± 0.264	1.093 ± 0.511	Rayleigh
Vertical Velocity (FFB)	M_Z^{FUR}	1.095 ± 0.259	1.09 ± 0.502	Rayleigh

Table 2. Magnitude scales and derived constants with 95% confidence intervals for observations at instruments RLAS, WET (Wettzell, Germany) and FUR (Fürstenfeldbruck, Germany), for equations of the form $M = \log_{10}(V/2\pi) + B \cdot \log_{10}(\Delta) + C$. The final column gives consideration to the wave type that each instrument component should provide a proxy for.

Scale	Label	B	C	Wave
Synthetic Rotation	M_{RT}^{SYN}	1.204 ± 0.086	3.841 ± 0.159	Love
Synthetic Rotation Rate	M_{RR}^{SYN}	1.215 ± 0.086	4.007 ± 0.161	Love
Synthetic Transverse Velocity	M_T^{SYN}	1.094 ± 0.081	0.146 ± 0.16	Love
Synthetic Vertical Velocity	M_Z^{SYN}	1.206 ± 0.08	-0.011 ± 0.149	Rayleigh

Table 3. Same as Table 2, but for magnitude scales derived with synthetic seismograms.

also because they provide the quickest method for determining earthquake size, requiring only measurements of amplitude and distance, useful for things like earthquake and tsunami early warning. Previous literature has recommended that the surface wave magnitude scale should be amended in the face of having a potential distance bias. In this study we report the same findings, and also recommend that use of the surface wave magnitude equation in its current form should be done with caution, and considerations for distance biases and component used for derivation of surface wave magnitude should be made.

Synthetic results prove drastically different from those predicted by observations, and warrants the doubt whether our synthetics contain the detail necessary to fully capture the reality of an earth structure which strongly affects amplitudes of surface waves. 3D crust and mantle models, including topography and a host of other factors that play a role in surface wave amplitudes, still predicted amplitudes one order of magnitude larger than those observed at our stations. Considerations should be made for the lack of realistic sources, however order of magnitude discrepancies seem too large to pin on a single problem. This large discrepancy points to a need for a more detailed and realistic full earth model than what is available at this time, if it is to be used for this purpose of determining correct amplitudes.

Many questions arose from analysis of these results which require further investigation, but fall outside the scope of this paper. One such question is where the discrepancy between observed rotation and translation amplitude decays arises from. If this effect is a factor of the wavetypes our instruments are sensitive to: what, theoretically, causes the difference in decay rates between Love waves and Rayleigh waves? Is this detectable in other regions and tectonic settings, or only seen for stations on the European continent? Perhaps this magnitude scale analysis could be performed only for transverse, radial and vertical components of single stations, to see if these values of B and C are recovered in other areas. In regards to the synthetics, what sort of modifications to our earth models are required to reproduce the effects we are seeing with our observations? If point sources are insufficient in producing the teleseismic amplitudes we observe, what level of complexity is required to accurately model waves at these periods and distances? In the same vein, how important is the observational setup; does the number of stations, receivers and station-receiver pairs have a strong impact on the values we recover? Would an observational setup with hundreds of sensors and events provide a different perspective than what we have seen here? Finally in regards to a rotation based magnitude scale; if we are observing such large differences between rotation and vertical velocity based magnitude scales, this might warrant defining a new magnitude scale solely for Love waves. Ground motion from these Love and Rayleigh waves are starkly different and perhaps one single surface wave magnitude scale is insufficient. If these discrepancies show up also in previous literature, perhaps it is necessary to instead define M_S^{LOVE} and $M_S^{RAYLEIGH}$ to replace the current M_S^{BB} . At the time of writing, with the push for field deployable rotation sensors and with an increasing number of rotation observations available, it would be possible to quickly determine peak amplitudes of rotations for incoming surface waves and define some magnitude based on an instrument only sensitive

to Love waves. If this is the case, we propose in this study that the current rotation based magnitude scale given in Table 2 should be used as a preliminary Rotation magnitude scale for determining magnitudes of events for instruments measuring rotation on the vertical axis. We expect further observations, instruments and seismic events can be used to refine these preliminary values.

A lack of observations at epicentral distances less than 20° and greater than 140° provides large uncertainties in the accuracy of our rotation magnitude scale. Going forward, it would be immensely beneficial to collect peak amplitude values at these distances to provide further constraint on our magnitude scales. The inclusion of more stations recording the same event would also make these derived scales much more robust. Since it may be a some time before full networks of permanent six component stations are available, inclusion of array derived rotations would prove the most useful method in providing more data for determination of these magnitude scales. For synthetics, deeper exploration of individual waveforms might assist in understanding where our current global models fail in accurately recreating real world observations.

Measurements of rotations and spatial gradients has proven a very interesting theoretical aspect of a field which has become extremely proficient in stable observations of three translational components. With this new observable, we are able to revisit theories, proposed decades before, with a new perspective. With the development of translational and rotational magnitude scales, we have determined some stark differences in observed amplitude decays between these two observables, and believe we can put forth the idea that Love waves exhibit stronger observed amplitude decays compared to Rayleigh waves, and that perhaps it is necessary to split our current definition of surface wave magnitude into two definitive definitions. Time will tell whether these results hold, as rotation measurements become more readily available and accessible, however it is exciting to see how these might change as a new slew of instruments and observations become available to the field of seismology.

REFERENCES

- Aki, K. and Richards, P. G. (2002). *Quantitative seismology*.
 Ambraseys, N. and Free, M. (1997). Surface-wave magnitude calibration for european region earthquakes. *Journal of Earthquake Engineering*, 1(01):1–22.
 Bassin, C., Laske, G., and Masters, G. (2000). The current limits of resolution for surface wave tomography in North America. *EOS Trans. Am. Geophys. Union*, 81(48):F897. Fall Meet. Suppl., Abstract S12A-03.
 Bernauer, F., Wassermann, J., Guattari, F., Frenois, A., Bigeur, A., Gaillot, A., de Toldi, E., Ponceau, D., Schreiber, U., and Igel, H. (2018). Blueseis3a: Full characterization of a 3c broadband rotational seismometer. *Seismological Research Letters*.
 Bormann, P. and Bergman, E. (2000). The new iasp91 manual of seismological observatory practice. *Seismological Research Letters*, 71(5):510–518.
 Donner, S., Lin, C.-J., Hadzioannou, C., Gebauer, A., Vernon, F., Agnew, D. C., Igel, H., Schreiber, U., and Wassermann, J. (2017). Comparing direct observation of strain, rotation, and displacement with array estimates at piñon flat observatory, california. *Seismological Research Letters*, 88(4):1107–1116.
 Ekström, G., Nettles, M., and Dziewoński, A. (2012). The global

- cmt project 2004–2010: Centroid-moment tensors for 13,017 earthquakes. *Physics of the Earth and Planetary Interiors*, 200:1–9.
- Herak, M. and Herak, D. (1993). Distance dependence of ms and calibrating function for 20 second rayleigh waves. *Bulletin of the Seismological Society of America*, 83(6):1881–1892.
- Igel, H., Cochard, A., Wassermann, J., Flaws, A., Schreiber, U., Velikoseltsev, A., and Pham Dinh, N. (2007). Broad-band observations of earthquake-induced rotational ground motions. *Geophysical Journal International*, 168(1):182–196.
- Igel, H., Schreiber, U., Flaws, A., Schuberth, B., Velikoseltsev, A., and Cochard, A. (2005). Rotational motions induced by the m8. 1 tokachi-oki earthquake, september 25, 2003. *Geophysical research letters*, 32(8).
- Karnik, V., Kondorskaya, N., Riznitchenko, J. V., Savarensky, E., Soloviev, S., Shebalin, N., Vanek, J., and Zatopek, A. (1962). Standardization of the earthquake magnitude scale. *Studia Geophysica et Geodaetica*, 6(1):41–48.
- Komatitsch, D. and Tromp, J. (2002a). Spectral-element simulations of global seismic wave propagation?i. validation. *Geophysical Journal International*, 149(2):390–412.
- Komatitsch, D. and Tromp, J. (2002b). Spectral-element simulations of global seismic wave propagation?ii. three-dimensional models, oceans, rotation and self-gravitation. *Geophysical Journal International*, 150(1):303–318.
- McLeod, D., Stedman, G., Webb, T., and Schreiber, U. (1998). Comparison of standard and ring laser rotational seismograms. *Bulletin of the Seismological Society of America*, 88(6):1495–1503.
- Rial, J. A., Saltzman, N. G., and Ling, H. (1992). Earthquake-induced resonance in sedimentary basins. *American Scientist*, 80(6):566–578.
- Ritsema, J., Deuss, A., van Heijst, H. J., and Woodhouse, J. H. S40rts: a degree?40 shear?velocity model for the mantle from new rayleigh wave dispersion, teleseismic traveltimes and normal?mode splitting function measurements. *Geophysical Journal International*, 184(3):1223–1236.
- Salvermoser, J., Hadzioannou, C., Hable, S., Krischer, L., Chow, B., Ramos, C., Wassermann, J., Schreiber, U., Gebauer, A., and Igel, H. (2017). An event database for rotational seismology. *Seismological Research Letters*, 88(3):935–941.
- Sbaa, S., Hollender, F., Perron, V., Imtiaz, A., Bard, P.-Y., Mariscal, A., Cochard, A., and Dujardin, A. (2017). Analysis of rotation sensor data from the sinaps@ kefalonia (greece) post-seismic experiment?link to surface geology and wavefield characteristics. *Earth, Planets and Space*, 69(1):124.
- Schreiber, K. U., Stedman, G. E., Igel, H., and Flaws, A. (2006a). Ring laser gyroscopes as rotation sensors for seismic wave studies. In *Earthquake source asymmetry, structural media and rotation effects*, pages 377–390. Springer.
- Schreiber, U., Igel, H., Cochard, A., Velikoseltsev, A., Flaws, A., Schuberth, B., Drewitz, W., and Müller, F. (2006b). The geosensor project: rotationsa new observable for seismology. In *Observation of the Earth System from Space*, pages 427–443. Springer.
- Shearer, P. M. (2009). *Introduction to seismology*. Cambridge University Press.
- Spudich, P., Steck, L. K., Hellweg, M., Fletcher, J., and Baker, L. M. (1995). Transient stresses at parkfield, california, produced by the m 7.4 landers earthquake of june 28, 1992: Observations from the upsr dense seismograph array. *Journal of Geophysical Research: Solid Earth*, 100(B1):675–690.
- Stedman, G. (1997). Ring-laser tests of fundamental physics and geophysics. *Reports on progress in physics*, 60(6):615.
- Stein, S. and Wysession, M. (2009). *An introduction to seismology, earthquakes, and earth structure*. John Wiley & Sons.
- Tanimoto, T., Hadzioannou, C., Igel, H., Wassermann, J., Schreiber, U., Gebauer, A., and Chow, B. (2016). Seasonal variations in the rayleigh-to-love wave ratio in the secondary microseism from colocated ring laser and seismograph. *Journal of Geophysical Research: Solid Earth*, 121(4):2447–2459.